Effect of Electron Temperature and Impact Ionization on Martian Return AOTV Flowfields

Leland A. Carlson* and Thomas A. Gally†
Texas A&M University, College Station, Texas 77843

Various electron impact ionization models in conjunction with a quasiequilibrium electron temperature model have been investigated and applied to the stagnation region of a hypothetical 2.3-m nose radius Martian return aeroassisted orbital transfer vehicle (AOTV). For the conditions considered, $U = 12$ km/s at 80 km, both multitemperature inviscid and viscous results indicate that a two-step ionization impact model predicts ionization distances in agreement with experimental data, that nonequilibrium chemistry and radiation effects are important throughout the stagnation zone, and that the quasiequilibrium electron temperature model is reasonable. Also, using a nongray emission-absorption radiation step model, it is shown that nonequilibrium causes a reduction in radiative heating from that predicted for equilibrium conditions and that, compared to an adiabatic wall, a cool wall (1650 K) results in a 28–45% reduction in radiative heating due to absorption near the wall.

Introduction

In the future, various space programs will be conducted that will require the efficient return of large payloads to low Earth orbit (LEO) from missions to the moon or planets such as Mars. To accomplish this task, the return vehicles will utilize aerocapture techniques that will involve re-entry and deceleration at high altitudes, and to design these vehicles, a thorough understanding of the physical phenomena will be required. Because of the high altitudes associated with aerocapture, the vehicle flowfields will be dominated by chemical, thermal, and radiative nonequilibrium phenomena, which in many cases have not been extensively studied since the Apollo era.[1] Recently, as a result of the Aeroassisted Flight Experiment (AFE) program, results have been presented for aerocapture flowfields in the range of 7.5–10 km/s (Refs. 2–7). These results have demonstrated the importance of nonequilibrium phenomena in this flight regime.

However, for a Martian return vehicle the minimum nominal Earth entry velocity is approximately 12 km/s and the vehicle might be required under certain conditions to be able to operate and survive at Earth entry speeds up to 16 km/s.[8] At these higher velocities, the nonequilibrium phenomena will be different from those associated with the AFE vehicle. In the stagnation region, for example, nonequilibrium should be dominated by electron impact ionization processes instead of dissociation reactions; extensive thermal nonequilibrium involving at least three temperatures (heavy particle, vibrational, and electron) will exist; and the radiative heat transfer may be significantly affected by local thermodynamic nonequilibrium or nonequilibrium radiation effects. In addition, the electron temperature and nonequilibrium chemistry will be strongly coupled, and this coupling will influence the radiative heat transfer to the vehicle. Furthermore, at the higher end of the velocity range (14–16 km/s), the radiative transfer and the flowfield gasdynamics will be coupled due to the significant energy losses associated with radiation cooling.

Currently, several different engineering models and reaction rates have been postulated for electron impact ionization chemistry, all of which depend on the accurate prediction of electron temperature. The purpose of the present effort is to examine these different electron impact ionization models using flowfield results obtained from both inviscid and viscous, nonequilibrium chemistry, multitemperature computational models. By comparing the results with each other, the consequences of using a specific model can be determined. Furthermore, by comparing these results with experimental data, a suitable ionization model for the stagnation region can be determined.

Problem Formulation

Flowfield Models

In this study both inviscid and viscous flowfield representations have been utilized. For the inviscid calculations an improved version of a previously developed[6] nonequilibrium chemistry axisymmetric inverse method based on the work of Grosse[9] has been utilized as the basic Euler equation flow solver. This method permits arbitrary chemistry, includes options for a variety of vibration dissociation coupling models, and, in the computation of radiative transfer, accounts for nongray gas spectral and local thermodynamic nonequilibrium phenomena. For the present effort it has been further modified to include an electron temperature model and both one- and two-step atomic ionization models.

Since at the high altitudes and low densities of interest in aerocapture both viscous phenomena and wall thermal boundary-layer effects will be important, calculations have also been obtained using a modified version of the NASA Langley nonequilibrium chemistry viscous shock-layer code VSL3DNQ, which is an axisymmetric version of the SHTNEQ code described in Ref. 10. Like the inviscid code, this viscous shock-layer (VSL) method has also been modified to include an electron temperature model and both one- and two-step atomic ionization formulations. In addition, it has been combined with a nongray emission-absorption radiation model to permit the computation of radiative heat transfer. However, the effects of radiation gasdynamic coupling due to radiation cooling have not yet been included in the VSL formulation.

Presented as Paper 89-1729 at the AIAA 24th Thermophysics Conference, Buffalo, NY, June 12–14, 1989; received July 13, 1989; revision received Dec. 18, 1989.

*Professor, Department of Aerospace Engineering. Associate Fellow AIAA.

†Research Assistant, Department of Aerospace Engineering. Student Member AIAA.

Electron Impact Ionization

At conditions of interest for Earth return from Mars, the nonequilibrium chemistry region behind the bow shock will be dominated by ionization chemistry. Initially, ions will be produced via reactions involving NO^+ and N_2^+ and precursor photoionization, but once significant dissociation has occurred and reasonable amounts of atomic nitrogen and oxygen are present, the atoms will directly ionize in collisional reactions. Of these the most important are the electron impact reactions:

$$N + e^- = N^+ + e^- + e^- \quad (1a)$$

$$O + e^- = O^+ + e^- + e^- \quad (1b)$$

since they can induce electron avalanche and, thus, strongly affect the length and character of the nonequilibrium zone.

The classical model for these reactions uses standard forms for the species production terms, reaction rates, and equilibrium constant. This approach essentially assumes that the ionization mechanism proceeds via a one-step process, and a widely used set of reaction rates for these reactions consists of the following:

For $N + e^- = N^+ + e^- + e^-$,

$$k_f = 1.1 \times 10^{32} T_e^{-3.14} \exp(-169{,}000/T_e) \quad (2)$$

$$k_b = 2.2 \times 10^{40} T_e^{-4.5} \quad (3)$$

where k_f and k_b are the forward and reverse rate coefficients based on the local electron temperature T_e.

For $O + e^- = O^+ + e^- + e^-$,

$$k_f = 3.6 \times 10^{31} T_e^{-2.91} \exp(-158{,}000/T_e) \quad (4)$$

$$k_b = 2.2 \times 10^{40} T_e^{-4.5} \quad (5)$$

Following normal practice, it is assumed that in these reactions the governing temperatures are the electron temperatures. These rates were presented by Kang et al.[11] as part of an extensive reaction chemistry set, and results using this set yielded good agreement with electron probe measurements on the flank region of the RAM-C flight vehicle experiment. Both recombination coefficients, Eqs. (3) and (5), have the form resulting from elementary[12] and variational theory three-body collision theory,[13] and the coefficient is near the upper bound determined by Makin and Keck.[13] In fact, several figures in Ref. 11 are labeled "Results are for upper-bound reaction rate coefficients for de-ionization reactions."

Similar recombination rates were also used in reflected shock-tunnel nozzle flow investigations of C^+ recombination and O_2^+ and N_2^+ dissociative recombination in which good results were obtained.[14-16] However, as noted by the investigators, these experiments may not have been sensitive to these reactions since in one case the leading coefficient in Eq. (3) was varied by plus and minus two orders of magnitude with no effect on the data.[16] Also, these laboratory and flight experiments were for flows dominated by recombination and at lower electron densities and temperatures (2500–8000 K) than those that are of interest in the current investigation. Thus, although not establishing the validity of these rates for the present conditions, these experiments do not indicate that they are incorrect.

However, Park[17,18] measured the nitrogen ionic recombination rate at a nominal temperature of 10,000 K using an arc plasma wind tunnel and obtained values that corresponded to a recombination rate of

$$k_b = 5.02 \times 10^{42} T_e^{-5.27} \quad (6)$$

which is in reasonable agreement with the value of Kang et al.[11] He also suggested that the forward rate be obtained from the equilibrium constant, K_{eq}, via

$$K_{eq} = k_f / k_b \quad (7)$$

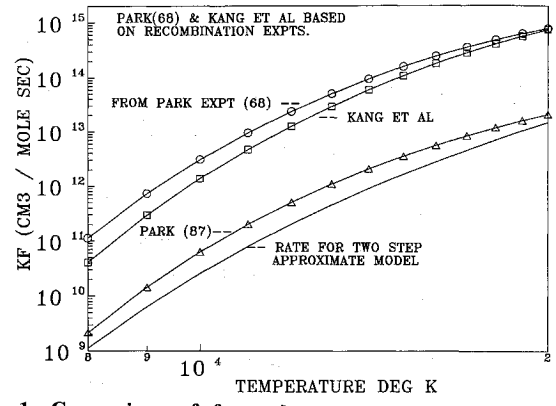

Fig. 1 Comparison of forward rate constants for $N + e^- = N^+ + e^- + e^-$.

Both the Park forward rate corresponding to Eq. (6) and the Kang et al. forward rate given in Eq. (2) are plotted in Fig. 1. As can be seen, the agreement between the two rates over the range of electron temperatures of interest in the present study is good.

Now it should be recognized that, for the high temperatures of interest in the present effort, three-body deionization recombination will include significant electron capture into low-lying levels and collisional de-excitation should be rapid.[12] In addition, although the atomic electronic excited state populations may be in a Boltzmann distribution during recombination [i.e., local thermodynamic equilibrium (LTE)], at T_e, experimental evidence[19] indicates that many of the excited state population densities may not be in equilibrium with the number density of free electrons. As will be discussed later, this nonequilibrium with the free electrons during recombination is in contrast with the behavior that can be assumed to occur behind a shock wave during ionization.

Recently, Park[4] used a two-temperature ionizing air model and obtained good agreement with shock-tube, shock-tunnel, and flight measurements of phenomena immediately behind a shock front and/or in the stagnation zone and forward face region of blunt bodies. For these studies several of the reaction rates were adjusted in order to yield good comparisons with experimental data, and the forward rates for the reactions in Eq. (1) are considerably different from those given by Eqs. (2–7). These rates consist of the following:

For $N + e^- = N^+ + e^- + e^-$,

$$k_f = 2.5 \times 10^{33} T_e^{-3.82} \exp(-168{,}600/T_e) \quad (8)$$

For $O + e^- = O^+ + e^- + e^-$,

$$k_f = 3.9 \times 10^{33} T_e^{-3.78} \exp(-158{,}500/T_e) \quad (9)$$

and the forward rate for atomic nitrogen electron impact ionization is plotted in Fig. 1. Note that it is almost two orders of magnitude smaller than the rates based on recombination.

The second model for atomic ionization is an engineering approximation based on various theories involving the ionization of argon[20-24] and the application of these theories to nitrogen and oxygen.[25,26] This approach assumes that atomic ionization is not a one-step process but proceeds via a two-step chain involving excitation to an excited state followed by rapid ionization controlled by the local charged particle concentrations and the electron temperature. This concept applies not only to electron impact ionization but also to heavy particle ionization involving atom-atom and atom-ion collisions.

Unfortunately, because of the two-step process, the usual mass production rate formulation is not completely adequate.

For example, assume that the atom-atom ionization process proceeds as follows:

$$N_g + M = N^* + M \tag{10}$$

$$N^* = N^+ + e^- \tag{11}$$

where N* refers to atomic nitrogen in an excited state. By assuming that the first step is rate determining, that dN^*/dt is approximately zero, and that the ground state concentration approximately equals the atom concentration, kinetics yields the rate of species mass production per unit volume $\dot{\omega}_s$ to be

$$\dot{\omega}_{N^*,\,\text{total}} = \mathfrak{M}_N\{k_f[N_g][M] - k_b[N^*][M]\} + \dot{\omega}_{N^*,11} \tag{12}$$

where k_f and k_r are for Eq. (10), brackets denote concentration, $\mathfrak{M}_s$ is the molecular weight of species s, and the subscript 11 refers to Eq. (11). However, by assumption,

$$\dot{\omega}_{N^*,\text{total}} = 0$$

so that

$$\dot{\omega}_{N^*,11} = -\mathfrak{M}_N\{k_f[N_g][M] - k_b[N^*][M]\} \tag{13}$$

But k_f and k_r are related by the equilibrium constant for Eq. (10):

$$K_{eq} = \frac{g^* \exp(-E^*/kT)}{g_g} = \frac{k_f}{k_b}$$

where g is the degeneracy of the indicated energy level E, and k is the Boltzmann constant. Thus, Eq. (13) becomes

$$\dot{\omega}_{N^*,11} = -\mathfrak{M}_N k_f[N_g][M]\left\{1 - \frac{g_g \exp(E^*/kT)[N^*]}{g^*[N_g]}\right\} \tag{14}$$

At this point, a rate expression relating the excited state to the ions and free electrons could be introduced instead. However, based on experimental evidence for monoatomic gases,[19,24] it can be assumed as an approximation that the excited states of nitrogen are in equilibrium with the free electrons and ions at the electron temperature. Thus,

$$\frac{N_e N_{N+}}{N_{N^*}} = \frac{Q_{N+}^{el} Q_{e-} \exp(-X/kT_e)}{g^*} \tag{15}$$

where X is the ionization potential from the excited state, Q_s^{el} is the electronic partition function of species s, and Q_{e-} is the partition function for the electrons defined by

$$Q_{e-} = 2\left(\frac{2\pi m_e kT_e}{h^2}\right)^{3/2}$$

where h is the Planck constant and m_e is the electron particle mass. Substituting Eq. (15) into Eq. (14) and noticing that

$$\dot{\omega}_{e,11} = (\mathfrak{M}_e/\mathfrak{M}_N)\dot{\omega}_{N^*,11}$$

yields, for $M = N$,

$$\dot{\omega}_{e,N} = \mathfrak{M}_e k_f[N]^2\left[1 - \frac{g_g \exp\left(\frac{E^*}{kT} + \frac{X}{kT_e}\right) AV[e^-][N^+]}{Q_{e-}Q_{N+}^{el}[N]}\right] \tag{16}$$

where AV is Avogadro's constant, and the subscript 11 is replaced by the incident particle for the two-step reaction, M.

A similar analysis for $M = N^+$ ionization yields

$$\dot{\omega}_{e,N+} = \mathfrak{M}_e k_f[N][N^+] \times\left[1 - \frac{Q_N^{el}\exp\left(\frac{E^*}{kT} + \frac{X}{kT_e}\right) AV[e^-][N^+]}{Q_{e-}Q_{N+}^{el}[N]}\right] \tag{17}$$

whereas, for electron impact ionization, $M = e^-$, the result is

$$\dot{\omega}_{e,e} = \mathfrak{M}_e k_f[N][e^-]\left[1 - \frac{g_g \exp\left(\frac{I}{kT_e}\right) AV[e^-][N^+]}{Q_{e-}Q_{N+}^{el}[N]}\right] \tag{18}$$

Similar expressions could be obtained for atomic oxygen ionization.

Notice that the production rates involving heavy particles (atoms and ions) are governed by both the electron and the heavy particle temperature, whereas the production rate for the atom-electron reactions involves only the electron temperature but has the classical form. Furthermore, the forward rate coefficient is for the limiting step and only uses the energy of the assumed excited state and not the ionization energy. Wilson,[25] using the work of Petschek and Byron,[27] assumed that the rate-limiting step in the ionization process was the excitation of the atoms to the level involving the largest energy jump, i.e., to the $3s^4P$ for nitrogen and to the $3s^5S$ state for oxygen, and they proposed a form for the excitation rate. It should be noted that for oxygen and nitrogen this rate-limiting step is for the temperatures of interest here and differs from that used in Ref. 13, which was only 2.5 eV below the ionization level.

Using this theory, Wilson obtained good agreement with shock-tube data for ionization distances behind shock waves in air. Subsequently, these forms were used to deduce rates that were used to study nonequilibrium radiating phenomena behind reflected shock waves[26] and the AFE stagnation region.[6]

Thus, based on the theory and results presented in Refs. 24–26, reaction rates consistent with the two-step approximate model given by Eqs. (10–18) consist of the following:

For $N + e^- = N^+ + e^- + e^-$,

$$k_f = 4.16 \times 10^{13} T_e^{0.5} \exp(-120{,}000/T_e) \tag{19}$$

For $O + e^- = O^+ + e^- + e^-$,

$$k_f = 5.49 \times 10^{13} T_e^{0.5} \exp(-104{,}500/T_e) \tag{20}$$

For $N + N = N^+ + e^- + N$ and $N + N^+ = N^+ + e^- + N^+$,

$$k_f = 2.34 \times 10^{11} T^{0.5} \exp(-120{,}000/T) \tag{21}$$

The forward rate given by Eq. (19) is also shown in Fig. 1 and is in reasonable agreement with the ionization rate of Park.[4] As can be seen, both of the rates associated with ionization processes are considerably slower than those deduced from recombination experiments and theory. However, the difference might be due to fundamental differences in the processes involved. In the shock-tube case the process is dominated by forward ionization, and in the rate derivation it was assumed that the excited states were in equilibrium with the free electrons and ions. In the shock- and arc-tunnel experiments, the chemistry is dominated by recombination, and, as mentioned earlier, there is experimental evidence[19] that during

recombination the excited states may not be in equilibrium with the free electrons.

Electron Temperature Model

Besides chemical nonequilibrium, it is possible for a partially ionized gas to have regions of thermal nonequilibrium between electrons and the other heavier species. Such thermal nonequilibrium occurs because the rate of energy exchange between electrons and heavy particles is very slow due to the large mass differences in the species, and it is characterized by different free electron and heavy particle temperatures. Since atomic ionization and radiative transfer are dependent on and strongly coupled to the electron temperature, accurate models for computing it are essential.

Over the years a variety of models for determining the electron temperature have been presented[4-6,20-23,26,28-33] that differ in detail, level of complexity, and ease of solution. All of these start from the equation representing conservation of electron energy, which can be written as

$$\frac{\mathrm{D}(\rho_e h_e)}{\mathrm{D}t} + \rho_e U_e \cdot \frac{\mathrm{D}(u)}{\mathrm{D}t} + \frac{\partial}{\partial r} \cdot q_e + \rho_e h_e \left(\frac{\partial}{\partial r} \cdot u \right) - \frac{\mathrm{D}(p_e)}{\mathrm{D}t} + [\tau_e] : \left[\frac{\partial}{\partial r} ; u \right] - N_e X_e \cdot U_e - \dot{\omega}_e \frac{u^2}{2} = \sum_{j=1}^{S} (\xi_{ej} + U_e \cdot P_{ej}) + Q_e \tag{22}$$

If Bremmstrahlung and viscous stress effects are ignored, this equation becomes, showing only one dimension for simplicity,

$$\rho_e u_e \frac{\partial h_e}{\partial x} - u \frac{\partial p_e}{\partial x} + \frac{\partial}{\partial x} \left(-\lambda_e \frac{\partial T_e}{\partial x} \right) + \frac{\partial}{\partial x} (\rho_e U_e h_e) + \dot{\omega}_e h_e - h_e \frac{\partial}{\partial x} (\rho_e U_e) - \dot{\omega}_e \frac{u^2}{2} = U_e \frac{\partial p_e}{\partial x} + \sum_{j=1}^{S} (\xi_{ej} + U_e P_{ej}) + Q_e \tag{23}$$

where the first term on the right side represents the effect of external forces and is obtained from the electron momentum equation; the second term accounts for the rate of energy gain by electrons due to elastic encounters because of thermal motion of the particles; the third term represents the energy gain resulting from elastic encounters because of the relative fluid motion of the electrons; and the last term represents energy change due to inelastic encounters. The velocity U_e is the electron diffusion velocity.

In the past, several investigators,[20-23,26] using the full electron energy equation, have obtained results which indicate that when significant ionization is present in the postshock nonequilibrium zone the electron temperature is essentially constant at a value 10–15% above the theoretical equilibrium temperature until the heavy particle temperature falls to that value. After that, the two temperatures are essentially the same. Obviously, the use of such a constant temperature would simplify the electron temperature calculations, and this approach has been used in approximate flowfield solutions[31,34] and was considered for the present study. However, preliminary calculations demonstrated the difficulty of selecting a priori an appropriate effective constant electron temperature, and this approach was abandoned.

Another approach successfully used in the past for AFE flowfields[4,6] is to assume that the nitrogen vibrational temperature and the electron temperature are equal and to combine the electron and vibrational energy equations. This method is based on experimental data[35] and theoretical calculations[4,5] which show that, near 7000 K, vibrational processes strongly influence the electron temperature. However, for the conditions of the present study, temperatures are normally above 10,000 K, dissociation occurs rapidly behind the shock front, and the concentration of N_2 is very low over most of the nonequilibrium zone. Thus, vibration electronic coupling should not be significant, and this approach was not utilized in the present study.

Another model that has been used in the past[32,33] is the "quasiequilibrium approximation," in which all derivative terms are neglected in the electron energy equation. If it is further assumed that the charge exchange cross section between atoms and ions is sufficient to ensure that they have the same diffusion velocity and, due to rapid dissociation, that the concentration of diatomic molecules is low over most of the shock layer, then diffusion terms can also be neglected. Thus, Eq. (23) becomes

$$\dot{\omega}_e h_e - \dot{\omega}_e \frac{u^2}{2} = \sum_{j=1}^{S} \xi_{ej} + Q_e \tag{24}$$

Since vibration electronic coupling has been neglected, the inelastic term Q_e is composed of effects due to chemical reactions involving electrons. When an electron is created by an electron-atom reaction, the electron that caused the ionization will lose energy equivalent to the ionization potential E_I plus the energy of the created electron, which on the average is, say, e_{av}. The original electrons will rapidly equilibrate by elastic collisions and will have collectively lost energy $E_I + e_{av}$. The equilibration between the original electrons and the newly created one will not affect the energy per unit volume since it only involves a transfer of energy from one particle to another. Thus, the net energy loss from an electron atom ionization process is E_I, and the total is $\dot{\omega}_{e,eA} E_I / m_e$.

Similarly, every time an atom-atom ionization occurs, an electron of average energy e_{AA} is created, and the total energy gain for these processes is $\dot{\omega}_{e,AA} e_{AA} / m_e$. This is also the case for atom-ion ionization. Thus,

$$Q_e = -\frac{\dot{\omega}_{e,eA} E_I}{m_e} + \frac{\dot{\omega}_{e,AA} e_{AA}}{m_e} + \frac{\dot{\omega}_{e,AI} e_{AI}}{m_e} \tag{25}$$

For the present conditions, however, the electron-atom process should be the dominant ionization mechanism and the last two terms should be negligible.[21,26] For the parts of the flowfield where the other reactions are important, the concentration of electrons should be low enough that any error resulting from neglecting them in Eq. (25) should be small. Thus, only the first term of Eq. (25) need be retained.

General forms for the elastic interaction terms have been derived using collision integral theory in Ref. 36. Since diffusion effects are ignored in the quasiequilibrium model, these interaction terms can be reduced to

$$\xi_{ej} = [(m_e T_e)^{1/2} / m_j] S_{ej} N_e N_j (1.03478 \times 10^{-23})(T - T_e) \tag{26}$$

where centimeter-gram-second units are assumed; terms involving m_e have been dropped relative to heavy particle masses; and S_{ej} is the collision cross section between electrons and species j.

By substituting Eqs. (25) and (26) into Eq. (24), dropping the small term involving u^2 and rearranging, an approximate equation for the free electron temperature is

$$T_e = T - \frac{1.23357 \times 10^{-10}}{T_e^{1/2} SX [e^-] m_e} \times \left(\dot{\omega}_{e,eN} E_{I_N} + \dot{\omega}_{e,eO} E_{I_O} + \dot{\omega}_e \frac{5}{2} k T_e \right) \tag{27}$$

where

$$SX = N_N S_{eN} + N_O S_{eO} + N_{N^+} S_{eN^+} + N_{eO^+} S_{eO^+} + \tfrac{1}{2}(N_{N_2} + N_{O_2}) S_{eM}$$

Note that this equation is nonlinear since the cross sections are functions of translational and electron temperature as well as concentrations and that the various production rates also depend on both temperatures. In the present study an iterative method for solving this equation has been developed and included in both the inviscid and viscous flowfield solvers.

Chemistry Models

Since the primary objective of the present effort is to use multitemperature flowfield models to investigate the effect of different impact ionization models, the reaction chemistry schemes have been kept as simple as possible. For air, the 10 species, 11 reaction model shown in Table 1 has been used. Although this scheme is not as complete as some others (Ref. 11, for example), it should be adequate for the present study. In addition, numerical experiments were conducted using for the nitrogen dissociation reaction a series of reaction rates that varied by several orders of magnitude. For the conditions investigated, no significant effects on the ionization processes were observed.

However, since the air model did not contain all possibilities, particularly with respect to dissociation and oxygen ionization, results have also been obtained assuming a pure nitrogen freestream. At the conditions of interest, nitrogen is a reasonable representation of nonequilibrium radiating air, and more details can be included using a smaller number of species and reactions. The nitrogen reaction chemistry set consisting of five species and eight reactions is shown in Table 2. Notice that charge exchange is included.

In general, with the exception of the atomic ionization reactions, the rates shown in Tables 1 and 2 are similar to those used by other investigators[3,6,26,33,35] and are in the form

$$k_{f,b} = AT^B \exp(-E/T)$$

As noted in the tables, computations involving the one-step ionization models and the rates in Eqs. (2–5) will be termed case 1, and those using the two-step ionization model and the rates in Eqs. (19) and (20) are case 2.

Vibration Dissociation Coupling

It is well established that, in general, vibration dissociation coupling strongly influences the dissociation of diatomic molecules.[4–6] However, at the temperatures and velocities associated with the present study, dissociation occurs rapidly, and the influence of vibration dissociation coupling on the ionization processes is small. To confirm this, numerical experiments were conducted with the inviscid flowfield model using vibrational equilibrium, coupled vibration-dissociation-vibration (CVDV) coupling, and modified CVDV (MCVDV) coupling, and no significant differences between the results regarding the ionization processes were observed. Consequently, in the inviscid flow solver, the MCVDV model developed in Ref. 6 has been used. This coupling model includes corrections to the Landau-Teller relaxation time correlation to prevent unrealistically short relaxation times at high temperatures and accounts for the diffusive nature of vibrational relaxation at high temperatures.[4]

In its original form the viscous shock-layer code, VSL3DNQ, did not contain any vibration dissociation coupling model. Since the inviscid studies indicated that, for conditions associated with Earth entry return from Mars, vibrational coupling effects were small, the VSL code has not been modified, and all viscous calculations have assumed vibrational equilibrium.

Radiation Model

At the lower velocities associated with the Earth return from Mars of an aeroassisted orbital transfer vehicle (AOTV), i.e., 12 km/s, radiative heat transfer and associated self-absorption effects should be important, but the total radiative losses from the flowfield should be sufficiently small so that there is not any significant radiative gasdynamic coupling. Thus, once a flowfield solution has been obtained for a given reaction chemistry system, the flowfield solution can be used to compute the body radiative heat transfer. In the present study, the tangent slab approximation has been used, the wall surface is assumed to be nonemitting and nonablating, and precursor effects are assumed negligible. Also, an eight-step nongray absorption coefficient model based on the work of Olstad[37] and similar to that used in Ref. 6 has been used. However, it has been modified to yield, under equilibrium conditions, results with respect to both magnitude and spectral distribution that in general agree with RADICAL, the NASA Langley version of a detailed radiation program documented in Ref. 38. Based on a series of calculations, these modifications consisted of a reduction in the effective absorption cross sections in the frequency range of 6.89–10.98 eV, which is composed not only of continuum radiation but also several important lines. This step model has yielded reasonable engineering results for AFE flowfields[6] and, in conjunction with an approximate flow solver, has correlated well with the Fire 2 flight experiment.[34]

A spectral comparison between stagnation-point radiative heating predictions obtained using the present eight-step model and RADICAL is shown in Fig. 2. These results were obtained using the viscous flow solver with 99 points between the shock and the wall, case 1 rates, and assuming an adiabatic wall, and almost the entire shock layer for this case was in chemical and thermal equilibrium. The presence of line contributions is evident in the RADICAL results by the tall narrow peaks on top of the continuum curves in the infrared (0–3.1 eV) and ultraviolet (8–12 eV). Since the radiative heating to the wall is the area under these curves, it can be seen that, in general, the two models agree quite well, and, in fact, the results are within 15% overall. [Note that the vacuum ultraviolet (VUV) band in the eight-step model that starts at 14.56 eV actually extends to 31 eV.] However, the eight-step model still does appear to slightly overpredict the heating in the range of 6.89–10.98 eV, and further improvements can probably still be made. Nevertheless, particularly when computational efficiency is considered, the modified eight-step absorption coefficient model should be adequate for engineering and comparison studies.

In addition, the present radiation model contains a method for computing approximate correction factors that account for the effects of local thermodynamic nonequilibrium (LTNE). Such LTNE can exist in the chemical nonequilibrium

Table 1 Air reaction system

Reaction		A	B	E	Direction
$O_2+M=2O$	$+M$	1.19×10^{21}	-1.5	59,380	Forward
$NO+M=N$	$+O+M$	5.18×10^{21}	-1.5	75,490	Forward
$N_2+M=2N$	$+M$	2.27×10^{21}	-1.5	0	Backward
$N+O_2=NO$	$+O$	1.00×10^{12}	0.5	3,120	Forward
$N_2+O=NO$	$+N$	7.00×10^{13}	0.0	38,016	Forward
$N+O=NO^+$	$+e^-$	1.80×10^{21}	-1.5	0	Backward
$N+N=N_2^+$	$+e^-$	1.40×10^{13}	0.0	67,800	Forward
$N+N=N$	$+N^++e^-$	2.34×10^{11}	0.5	120,000	Forward
$N+N^+=2N^+$	$+e^-$	2.34×10^{11}	0.5	120,000	Forward
$N+e^-=N^+$	$+2e^-$	Eqs. (2) and (3) for case 1, (19) for case 2			
$O+e^-=O^+$	$+2e^-$	Eqs. (4) and (5) for case 1, (20) for case 2			

Table 2 Nitrogen reaction system

Reaction		A	B	E	Direction
$N_2+N_2=2N$	$+N_2$	4.70×10^{17}	-0.5	113,000	Forward
$N_2+N=2N$	$+N$	4.085×10^{22}	-1.5	113,000	Forward
$N_2+M=2N$	$+M$	1.90×10^{17}	-0.5	113,000	Forward
$N_2+N^+=N_2^+$	$+N$	2.02×10^{11}	0.8	13,000	Forward
$N+N=N_2^+$	$+e^-$	1.40×10^{13}	0.0	67,800	Forward
$N+N=N$	$+N^++e^-$	2.34×10^{11}	0.5	120,000	Forward
$N+N^+=2N^+$	$+e^-$	2.34×10^{11}	0.5	120,000	Forward
$N+e^-=N^+$	$+2e^-$	Eqs. (2) and (3) for case 1, (19) for case 2			

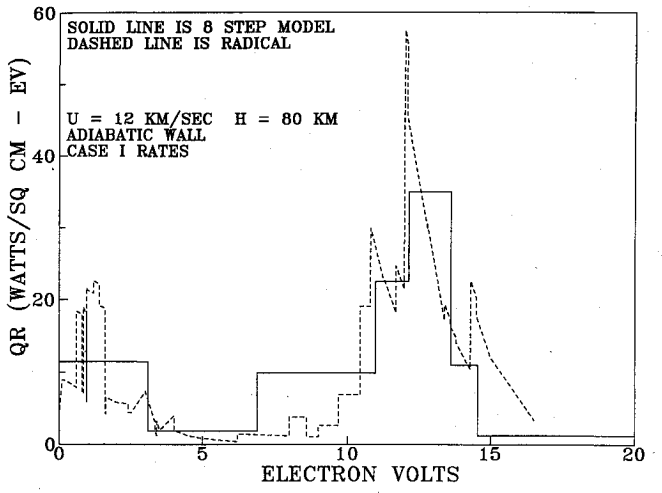

Fig. 2 Stagnation-point radiative heat transfer from RADICAL and eight-step model.

region immediately behind the shock front where, due to ionization via excited states, the populations of the electronic states may not be that predicted by an LTE assumption using the ground state. The rationale behind these factors and their derivation has been presented in Refs. 6 and 34, and similar factors have been used for monoatomic gases.[20–23] The inclusion of radiation nonequilibrium effects is essential for accurately predicting radiative heat transfer at high-altitude conditions.[4–6,34]

Originally, these LTNE factors were expressed in terms of the degree of dissociation and ionization,[6,34] which were often difficult to compute accurately. However, Greendyke[39] has pointed out that they can be more simply expressed in terms of the partition functions. Thus, the atomic nitrogen LTNE correction factor can be written as

$$\frac{N_{N^+} N_e Q_N^{el} \exp(169{,}000/T_e)}{N_N Q_{N^+}^{el} Q_{e^-}} \tag{28}$$

For radiation processes involving the ground state, this factor is multiplied by the blackbody function for that region to yield the effective source function, and the absorption coefficient is unchanged. On the other hand, for processes involving excited states, the factor is multiplied by the absorption cross section to yield the effective absorption coefficient, and the source function for that spectral region is unchanged. Additional details are presented in Ref. 6, and similar forms can be obtained for molecular radiation.

For cases where the reaction chemistry set is such that an opposite rate is obtained from a forward or reverse rate in conjunction with an equilibrium coefficient computed from partition functions, the correction factor form given in Eq. (28) is appropriate. This situation is the case with the two-step ionization model, whose rates have been designated case 2. In other words, in that case the factor predicted by Eq. (28) will go to one as the flow approaches ionization equilibrium.

However, when the one-step ionization rates of Kang et al.[11] are used, case 1, the ionization equilibrium coefficient is determined by the ratio of the forward-to-reverse rates [Eqs. (2–5)] and not by partition functions. In that case the atomic nitrogen LTNE correction factor should be computed using

$$(N_{N^+} N_e)/N_N A V K_{eq} \tag{29}$$

and the equilibrium coefficient is given by

$$K_{eq} = k_f/k_b = 5 \times 10^{-9} T_e^{1.36} \exp(-169{,}000/T_e) \tag{30}$$

If this approach is not taken, the factors will not approach one as chemical equilibrium is approached, and ridiculous answers may result.

For viscous cases in which a cool wall is considered, recombination processes will dominate in the wall thermal layer, and, as mentioned earlier, there is evidence that during recombination the excited states may not be in equilibrium with the free electrons and ions and the electronic states may all be populated according to a Boltzmann distribution, i.e., in LTE with the ground state. Consequently, in the wall thermal layer, the radiation should be computed using the local electron temperature and nonequilibrium species concentrations, and the LTNE factors should not be used (or set to unity).

Discussion of Results

Inviscid and viscous results have been obtained for the stagnation region of a 2.3-m nose radius axisymmetric blunt body for a freestream velocity of 12 km/s at an altitude of 80 km. This condition was selected because it is within the range of possible Martian return trajectories, and yet the velocity is low enough that radiation losses should be minor, at the most a few percent, compared to the total flow energy. Thus, radiation cooling and gasdynamic coupling effects should be small. Each inviscid solution covers the region between the shock and the body and from the centerline up to 10 cm above the axis and is typically composed of over 10,000 computational points. Inviscid solutions using both air and nitrogen freestreams have been obtained. Viscous solutions have been obtained along the stagnation streamline for nitrogen freestreams for adiabatic and cool wall situations. In both cases the wall was assumed to be nonemitting and noncatalytic, and in the cool wall case the wall temperature was assumed to be 1650 K, which is representative of nonablating heat shield materials.

Inviscid Results

Although flowfield properties along 21 different streamlines in the stagnation region were actually computed, details will only be presented for streamline C, which crossed the shock front 1.5 cm above the axis. This streamline is shown in Fig. 3 as a solid line, along with several other streamlines, the shock front, and the body. Depending on the reaction chemistry system, streamline C was typically composed of 700–2000 spatial grid points.

Figure 4 shows air results obtained using the one-step ionization model with case 1 rates, the quasiequilibrium electron temperature model, and MCVDV vibration dissociation coupling. Although individual vibrational temperatures were computed for N_2, O_2, NO, NO^+, and N_2^+, for clarity they are not included on the plots. Immediately behind the shock front, the heavy particle temperature T is almost 70,000 K, whereas the electron temperature T_e is at the freestream value, 180.65 K. Initially, T_e rapidly rises to about 10,000 K, whereas the heavy particle temperature falls sharply due to the rapid

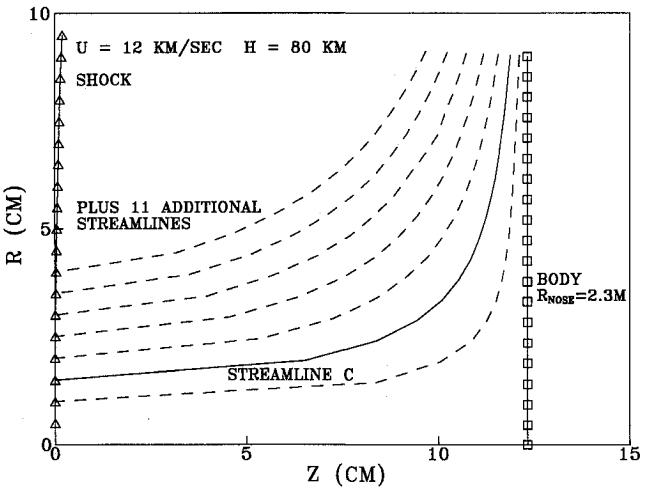

Fig. 3 Solution region for inviscid cases showing streamline C.

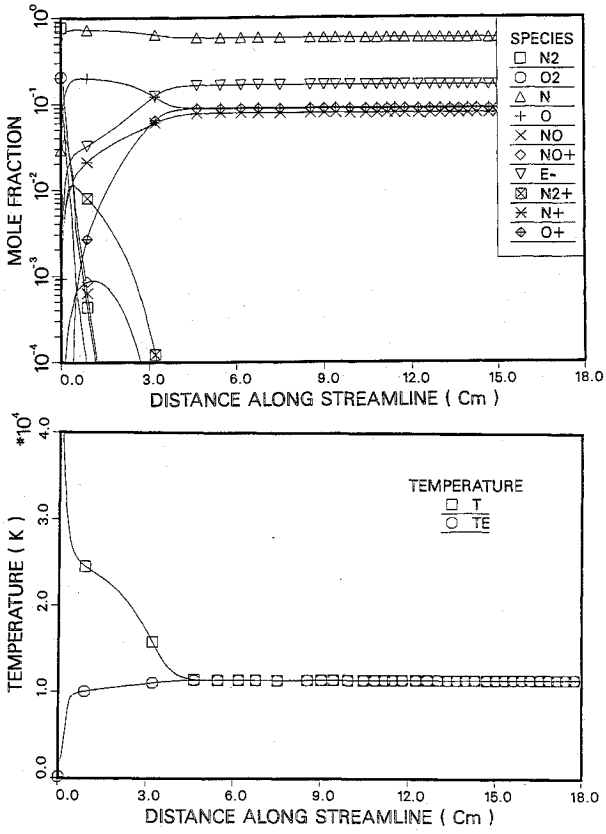

Fig. 4 Species and temperature profiles for air along streamline C, inviscid flow, case 1.

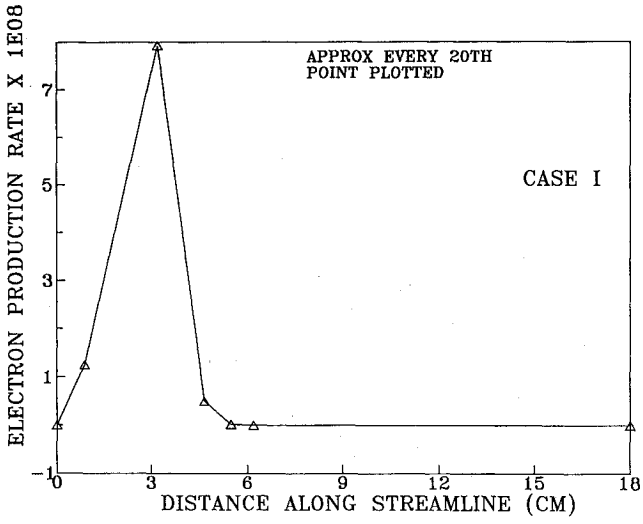

Fig. 5 Electron mass production rate along streamline C, inviscid case 1.

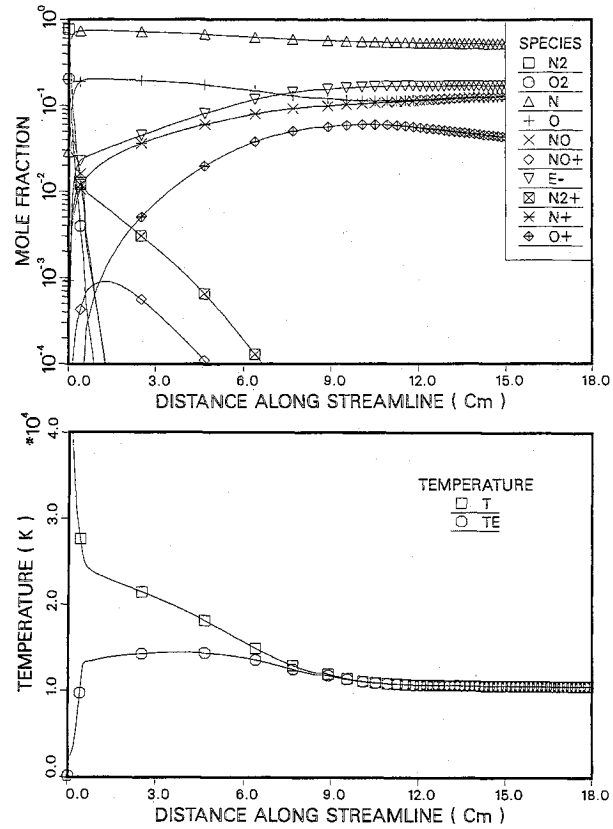

Fig. 6 Species and temperature profiles for air along streamline C, inviscid flow, case 2.

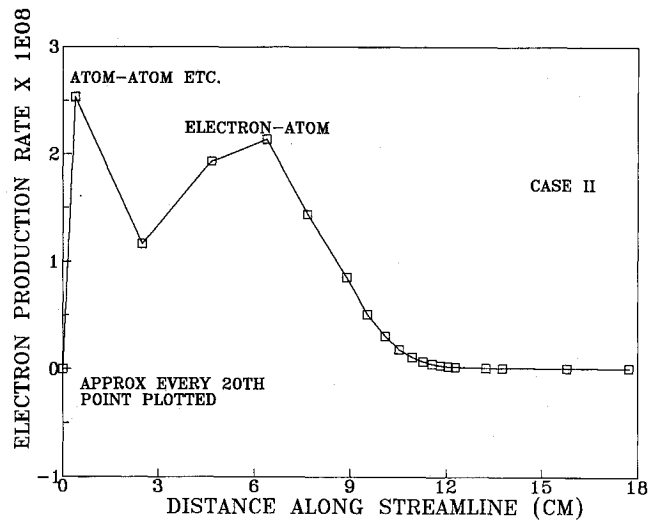

Fig. 7 Electron mass production rate along streamline C, inviscid case 2.

dissociation of N_2 and O_2. Subsequently, the electron temperature gradually increases until it equilibrates with the heavy particle temperature.

As can be seen on the concentration profiles, in the region immediately behind the shock front the concentration of atomic nitrogen and oxygen rises extremely rapidly, indicating that dissociation essentially occurs in the shock "front" as has been assumed in some approximate solutions.[25,34] Also N_2^+, NO, and NO^+ peak rapidly and essentially "disappear," and from a practical standpoint the entire nonequilibrium portion of the flowfield is dominated by atomic ionization. Interestingly, at the end of the equilibrium zone, the concentrations of N^+ and O^+ are similar. Furthermore, the heavy particle temperature and $[e^-]$ profiles exhibit a change in curvature around 2.5 cm, which is associated with the onset of electron avalanche from the electron impact ionization reactions.

The magnitude of this phenomena is shown in Fig. 5, which portrays the total electron production rate [in g/(cm^3-s)] for this case. Although the plot is somewhat lacking in detail since only approximately every twentieth point is plotted, it can be seen that avalanche starts at about 1 cm along the streamline. Apparently, by this point other ionization reactions have produced sufficient electrons, and the electron temperature has risen sufficiently to permit electron impact ionization to dominate. Both Figs. 4 and 5 indicate that for the case 1 rates the flow equilibrates in about 4.5 cm. It should be noted that the high electron production rate associated with the case 1 impact ionization rates prevents the free electron temperature from peaking and instead leads to its gradual rise until equilibrium is attained.

Inviscid results obtained using the two-step approximate ionization model with case 2 rates are shown for air in Figs. 6

and 7. The [N] and [O] profiles indicate rapid dissociation and are similar to those with the one-step model shown in Fig. 4. Likewise, the peak values for $[N_2^+]$ and $[NO^+]$ are similar but occur slightly later. The electron temperature initially rises to about 14,000 K, after which it remains relatively constant until it equilibrates with the heavy particle temperature. As can be seen by comparing the values in Figs. 7 and 5, the electron production rate for this case is significantly lower than that for the case 1 situation, and as a result the electron temperature is higher over most of the nonequilibrium region.

The biggest difference, however, between the case 1 and case 2 air results is in the behavior and length of the atomic ionization region. After the initial dissociation, the decrease in heavy particle temperature and increase in electron concentration is, by comparison, slow, and equilibrium is not achieved until 11 cm along the streamline. In addition, the $[N^+]$ concentration is significantly higher than the $[O^+]$ value. This latter difference is due to the fact that in this case the equilibrium composition is determined from the equilibrium coefficient computed by partition functions, whereas for the one-step case 1 rates it is specified by the ratio of the forward and reverse rates in Eqs. (2-5). At the present equilibrium temperatures, these two approaches yield equilibrium constants that differ by an order of magnitude, with resultant differences in final composition and temperatures.

In addition, Fig. 7 shows that the electron production rate for the two-step ionization model is different from that for the one-step case. Initially, electrons are created due to NO^+, N_2^+, atom-atom, and atom-ion reactions, and the production from these reactions rapidly peaks and then decreases. However, once $[e^-]$ becomes sufficiently high, electron-atom processes become important, the electron production rate increases, and electron avalanche occurs. However, since the two-step electron-atom ionization rate is less, the process is slower than in the one-step model and the time and distance to equilibrium is longer.

It is believed that these inviscid results demonstrate that predictions of ionization relaxation are strongly dependent on the atomic ionization model and the electron impact ionization rate.

Viscous Results

Using the nitrogen reaction chemistry set given in Table 2, viscous results have been obtained for the stagnation streamline with the modified VSL3DNQ code. In all cases, 99 points have been used between the shock front and the wall, and binary diffusion between molecular and atomic species has been included. Unlike the inviscid solver, which primarily used the partition function approach, the thermodynamic properties in the viscous solutions were computed using the curve fits presented by Gnoffo et al.[40]

Figure 8 shows temperature and concentration profiles for the cool wall case (T_ω = 1650 K) for the case 1 electron impact ionization rate. Notice that computational points have been clustered in the region immediately behind the shock front where nonequilibrium effects should be important and in the region near the wall where thermal and concentration gradients could be large. In the outer portion of the shock layer, these results are almost identical to the equivalent inviscid case in that dissociation is rapid behind the shock front, the electron temperature "peaks" and then gradually rises to equilibrate with the heavy particle temperature, and about two-thirds of the shock layer is in chemical equilibrium. In addition, the results show that the cool wall thermal layer affects about 20% of the shock layer and that in this region ion and molecular recombination processes are dominant. For this case the shock standoff distance was 11.8 cm and the computed convective heating rate to the noncatalytic wall was 46.7 W/cm^2.

Stagnation profiles for the two-step ionization model and the case 2 electron impact ionization are presented in Fig. 9. For the nonequilibrium zone behind the shock front, the dissociation is rapid and N_2^+ rapidly peaks and disappears; two-thirds or more of the shock layer is affected by ionization nonequilibrium relaxation. In addition, the relaxing temperature profile never reaches a constant plateau but smoothly merges into the wall thermal layer. For this case the shock detachment length was 12.0 cm and the convective heating was 44.4 W/cm^2.

The electron production rate for this cool wall case is presented in Fig. 10. Although there are some differences between this profile and the inviscid curve shown in Fig. 7 due to

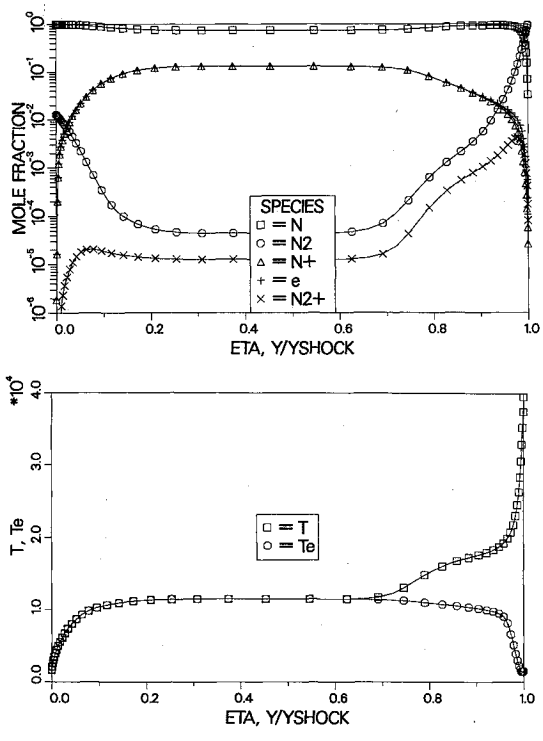

Fig. 8 Stagnation streamline species and temperature profiles, viscous case 1.

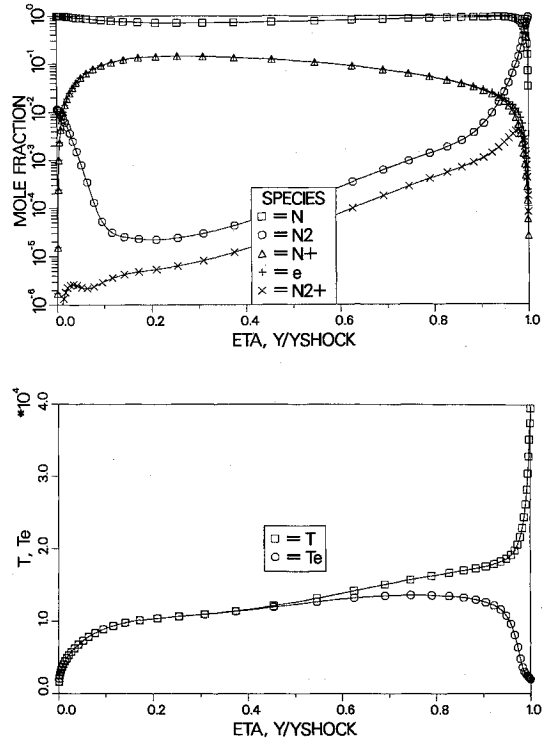

Fig. 9 Stagnation streamline species and temperature profiles, viscous case 2.

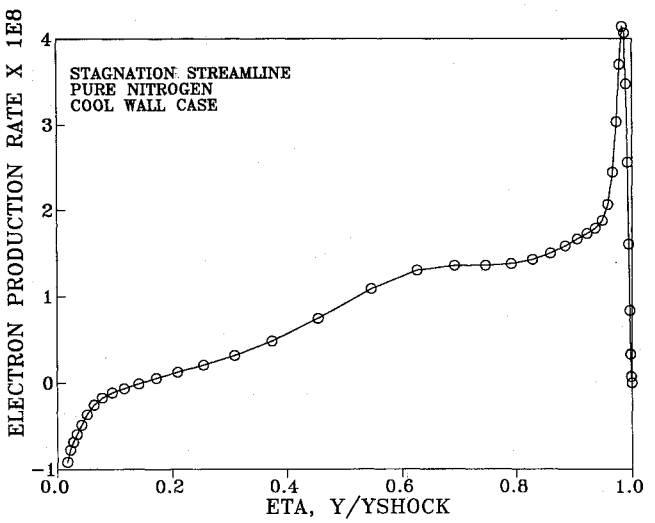

Fig. 10 Stagnation streamline electron mass production rate, viscous flow, case 2.

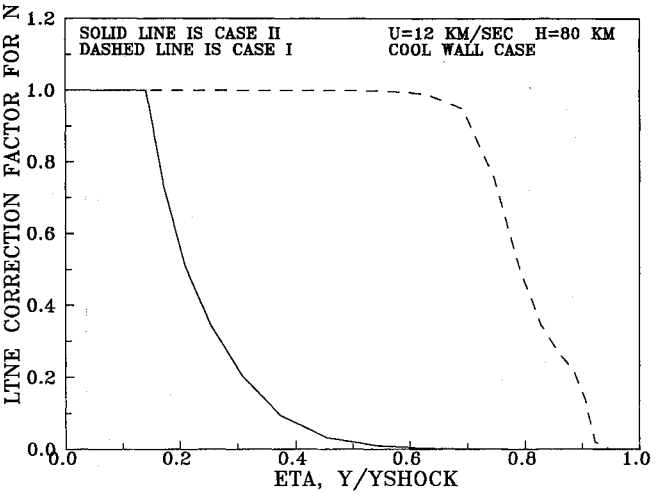

Fig. 11 Nonequilibrium radiation correction factors along stagnation streamline.

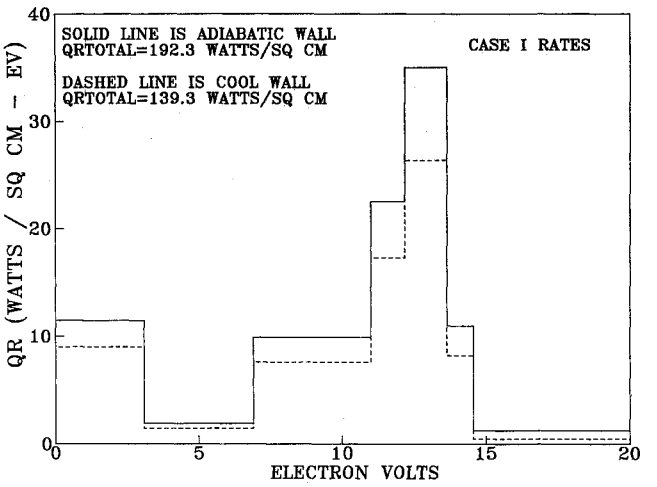

Fig. 12 Stagnation-point radiative heat transfer for case 1.

differences in velocity along and location of the streamlines, the overall pattern is similar. Initially, electron production is high due to N_2^+ ionization, atom-atom, and atom-ion reactions, and then it decreases. Subsequently, electron-atom ionization becomes important, as evidenced by the plateau around y/yshock of 0.8, followed by an approach toward equilibrium. Unlike Fig. 8, no second peak appears in the viscous profile, possibly due to diffusion effects and to the influence of the charge exchange reaction. Also, the electron production rate indicates that an equilibrium region is never achieved along the stagnation streamline, but that the flow simply transitions from an ionizing flow to one involving recombination (negative production rates) in the wall thermal layer.

Obviously, the different species concentration and temperature profiles between the case 1 and case 2 models and rates will greatly influence the predicted radiative heat transfer to the vehicle surface, since radiative heating depends on both electron temperature and species concentrations. However, it also depends on the extent of radiative nonequilibrium or the degree to which the excited state populations are depleted due to ionization. This nonequilibrium has previously been referred to as local thermodynamic nonequilibrium (LTNE) in the discussion concerning the radiation model, and it can be approximately accounted for via LTNE correction factors such as those in Eqs. (28) and (29).

Values for the correction factors for atomic nitrogen radiation are shown in Fig. 11 for both the case 1 and case 2 rates and models. For the one-step case 1 model, the correction factor is small in the chemical nonequilibrium zone, but then it rises rapidly and is essentially unity through the rest of the stagnation layer. Thus, for the one-step impact ionization model most of the shock layer is in local thermodynamic equilibrium radiatively. Similarly, the two-step case 2 factors are also very small in the chemical nonequilibrium zone, but they subsequently increase only slowly, and only very near the body in the wall thermal layer do they become one. Hence, for the case 2 flowfield, radiative nonequilibrium or LTNE effects are very important. Interestingly, when the approximate technique of Ref. 34 is applied to this case, it also predicts that most of the stagnation region is in LTNE.

In examining these results it should be realized that the two-step ionization chemistry and LTNE radiation models are approximate and are the most optimistic from the standpoint of reducing radiation and the rate of ionization, since they assume that the excited states are in equilibrium with the ions and free electrons. In actuality, the rate of ionization from the excited state, Eq. (11), may be finite, and the extent of LTNE indicated by the case 2 results on Fig. 11 may be less. Thus, the two sets of results in Fig. 11 could be viewed as bracketing the problem.

Stagnation-Point Radiative Heat Transfer

The viscous stagnation streamline nonequilibrium flowfields have been used to compute the radiative heat transfer to the wall. In all cases the wall has been assumed to be nonemitting and nonablating, and results have been obtained for both an adiabatic and the cool wall case. Considering the many factors involved in the current models, these radiative heating results should not be construed as definitive and should be used primarily for comparison purposes and model development until they have been verfied by more detailed models and/or experiments. Nevertheless, these results do include both the ultraviolet and the visible-infrared spectrum, emission and absorption phenomena, the variation of absorption coefficients with wavelength, chemical and thermal nonequilibrium, and radiative nonequilibrium. Thus, the present results include many effects not accounted for in other studies,[8] which assumed the gas cap to be in equilibrium and transparent and only included emission in the visible and infrared (IR) spectrum.

Figures 12 and 13 present stagnation-point radiative heat transfer for the present cases as a function of energy, and several significant points are evident. First, there is an order of magnitude difference in heat transfer both totally and in the individual spectral regions between the one-step case 1 flowfield and the two-step case 2 results. This difference is due to the larger chemical nonequilibrium region predicted by the

case 2 rates and the subsequent greater extent of the radiative nonequilibrium zone. Second, for both ionization models most of the radiation reaching the wall for the region below 6.89 eV (above 1800 Å), which is often referred to as the visible region since it is optically visible through quartz and sapphire windows, is in the region below 3.1 eV and is due to IR continuum and lines.

Third, the absorption effects of the cool wall thermal layer may not be as great as previously hoped.[5,8,33] With the present data, the effect of the wall thermal layer can be determined by comparing the cool wall results with the adiabatic wall values. For the case 1 situation in Fig. 12, lowering the wall temperature to 1650 K reduces the overall radiative heating 28%, and in the separate spectral bands the reduction is 22–25%, except for the VUV band from 14.56–31 eV. For that band the reduction is 61%, indicating that the far vacuum ultraviolet is extensively absorbed in the cool wall layer. Likewise, for the case 2 rates, Fig. 13 shows a reduction due to wall cooling of 46% in the total radiative heating. In this case, since the total input is considerably less than that for the one-step model, the thermal boundary layer has more of an effect. In the individual bands the reduction ranges from 39 to 44%, but again in the 14.56–31-eV VUV band the reduction is large (72%). Obviously, for both cases, although a cool wall significantly attenuates the far VUV and somewhat reduces the heating from other regions of the spectrum, significant radiative heat transfer still reaches the wall. This trend is consistent with previous approximate calculations at similar conditions.[34]

Fourth, there is significant radiative heat input to the wall from the spectral region above 6.89 eV (below 1801 Å). In fact, for both ionization models approximately 75% of the total radiative heating is from this region. This result is consistent with what has been observed and predicted for the Fire 2 experiment,[1,33,41] and it is also consistent with the shock-tube experiments of Wood et al.[42] Wood and co-workers conducted measurements with and without a quartz window and determined that 50–75% of the total radiant intensity was from the ultraviolet region of the spectrum. Interestingly, they also concluded from their experiments that a cool boundary layer would not absorb appreciably.

Comparison with Experimental Data

Based on the temperature, species, and radiative heat transfer profiles discussed earlier, it is apparent that the choice of ionization model and electron impact ionization rate greatly affects the resultant predictions, and it would be desirable to determine which model is more appropriate for blunt-body calculations. Although there is almost no radiation experimental data at the present velocity and pressure conditions, Wilson[25] did make measurements of the ionization rate of air behind shock waves having velocities between 9 and 12.5 km/s. By making IR measurements at around 6.1 μ, he was able to determine variations in electron density and thus the ionization relaxation distances.

Consequently, the concentration and temperature profiles for the present inviscid air data along streamline C have been used to compute theoretical IR emission profiles similar to those measured by Wilson for both the case 1 and case 2 models. These profiles are shown in Fig. 14 and have the same general shape as the signals measured by Wilson. Following his procedure the intercept with the equilibrium value of a line drawn through the maximum slope of the rising signal has been used to determine an ionization distance, denoted by the vertical dashed line on the figure, for each ionization model. Then the shock-tube data of Wilson have been used, accounting for differences in freestream pressure and for particle velocity differences behind a normal shock and along streamline C, to determine an experimental ionization distance for the present case. These distances are shown by the square symbols on Fig. 14. The center symbol is the nominal value, whereas the endpoints correspond to the data scatter and error band limits indicated in Ref. 25. As can be seen, the agreement between the shock-tube data and the prediction obtained using the two-step ionization model and the case 2 electron impact ionization rates is very good. Thus, it appears that a two-step ionization model in conjunction with ionization reaction rates based on forward processes should be used for the computation of nonequilibrium blunt-body flowfields associated with Earth aerocapture from Mars.

However, this conclusion does not mean that the ion recombination rates used by Kang et al.[11] or measured by Park[17] are in error. Unfortunately, there are many possible explanations for the observed differences. First, there could be an error in the experimental data[25] or its interpretation to the present problem. Second, at the current electron densities and temperatures, the results of Hinnov and Hirschberg[19] and of Bates et al.[43] indicate that the effective recombination rate is not strictly a function of electron temperature and that radiative recombination is still significant. Thus, the flow may not be totally collision-dominated. In such a situation, if a measured or effective reverse rate were used via an equilibrium constant to determine a forward rate, the resulting forward rate would be too large. As pointed out by Park,[18,44,45] the effective forward and reverse rates are only related via the equilibrium constant if the flow is collision-dominated. Third, there is the possibility[18] that, in the region immediately behind the shock front and due to the time scales involved, the forward and reverse rates are not related by the equilibrium constant and reasonable chemistry can only be predicted using a proper forward rate. Fourth, there exists the possibility that the elec-

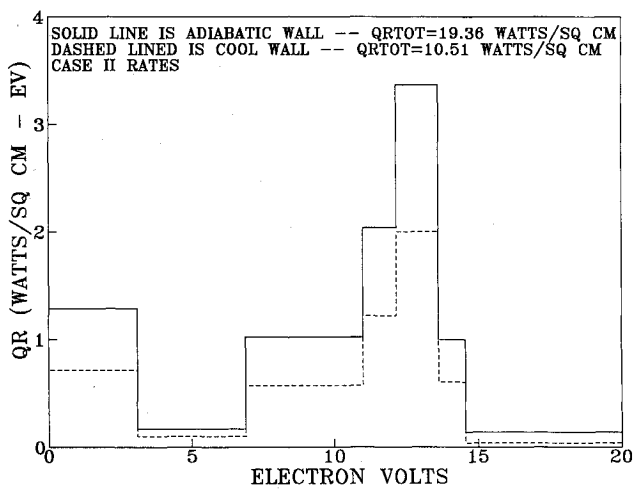

Fig. 13 Stagnation-point radiative heat transfer for case 2.

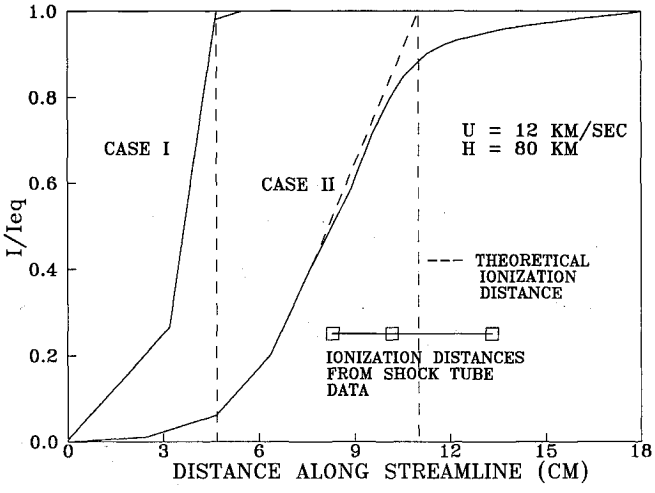

Fig. 14 Theoretical emission profiles and ionization distances for streamline C.

tronic temperatures are not in reality the same as the free electron temperature, and this fact requires the use of a different set of rates. A discussion of this situation and also of the details of atomic ionization are presented in Refs. 45 and 46. Finally, as mentioned previously, there exists the possibility that ionic recombination in a nozzle or arc tunnel is not the direct inverse of atomic ionization behind a shock wave. If anything, the present results indicate the difficulty of creating engineering models for these problems and the need for further analytical and experimental investigation. Nevertheless, based on the results presented here and the reaction rates discussed in Ref. 47, it is believed that the present two-step model with case 2 rates is appropriate for stagnation region computations.

Future Efforts

In the near future there are plans to continue these studies by developing a nonequilibrium radiation model based upon RADICAL. This new model will be incorporated into the VSL code along with radiation gasdynamic coupling. In addition, there exists a need to improve the ionization chemistry model and the LTNE correction factors by taking into account finite-rate processes between excited state atoms and ions. Also, there is a definite need for additional experimental data at velocities and pressures appropriate for a Mars return AOTV. This data should be for an ionizing, as opposed to a recombining, flow and probably could be obtained in a shock tube, although flight data would be desirable. Finally, the inclusion of preshock precursor, photoionization and recombination, and shock and wall slip effects would be desirable.

Conclusion

Based on the results presented, it appears that an approximate two-step ionization model in conjunction with quasiequilibrium electron temperature model is suitable for the computation of nonequilibrium blunt-body flowfields associated with Earth aerocapture from Mars. Also, nonequilibrium chemical and radiation effects are important at these conditions throughout the entire stagnation zone, and, compared to equilibrium predictions, these nonequilibrium phenomena can lead to a reduction in radiative heating. Furthermore, compared to an adiabatic wall, a cool wall results in a significant reduction in radiative heating due to absorption near the wall. However, the present results also indicate a need for further analytical and experimental investigations.

Acknowledgments

The authors gratefully acknowledge the assistance of the Associate Provost for Computing for providing a portion of the computational resources used in this effort. This work was initiated under a subportion of NASA Grant NAG 9-192 from the NASA Johnson Space Center (JSC). The authors thank the technical monitor, Carl Scott, Aerosciences Branch, JSC, for his suggestions, and Ken Sutton, Aerothermodynamics Branch, NASA Langley Research Center, for his comments and assistance in providing the RADICAL and VSL3DNQ programs. T. A. Gally is partially supported by a NASA Graduate Student Researchers Fellowship through the NASA Johnson Space Center.

References

[1]Sutton, K., "Air Radiation Revisited," *Progress in Astronautics and Aeronautics: Thermal Design of Aeroassisted Orbital Transfer Vehicles,* Vol. 96, edited by H. F. Nelson, AIAA, New York, 1985, pp. 419–441.

[2]Moss, J. N., Bird, G. A., and Dogra, V. K., "Nonequilibrium Thermal Radiation for an Aeroassist Flight Experiment Vehicle," AIAA Paper 88-0081, Jan. 1988.

[3]Gnoffo, P. A., and Green, F. A., "A Computational Study of the Flowfield Surrounding the Aeroassist Flight Experiment Vehicle," AIAA Paper 87-1575, June 1987.

[4]Park, C., "Assessment of Two Temperature Kinetic Model for Ionizing Air," AIAA Paper 87-1574, June 1987.

[5]Candler, G., and Park, C., "The Computation of Radiation from Nonequilibrium Hypersonic Flows," AIAA Paper 88-2678, June 1988.

[6]Carlson, L. A., Bobskill, G. J., and Greendyke, R. B., "Comparison of Vibration Dissociation Coupling and Radiative Heat Transfer Models for AOTV/AFE Flowfields," AIAA Paper 88-2673, June 1988.

[7]Li, C. P., and Wey, T.C., "Numerical Simulation of Hypersonic Flow Over an Aeroassist Flight Experiment Vehicle," AIAA Paper 88-2675, June 1988.

[8]Park, C., and Davies, C. B., "Aerothermodynamics of Manned Mars Mission," AIAA Paper 89-0313, Jan. 1989.

[9]Grosse, W. L., "A Thin Shock Layer Solution for Nonequilibrium, Inviscid Flows in Earth, Martian, and Venusian Atmospheres," NASA TN D-6529, Dec. 1971.

[10]Thompson, R. A., "Comparison of Nonequilibrium Viscous Shock Layer Solutions with Windward Surface Shuttle Heating Data," AIAA Paper 87-1473, June 1987.

[11]Kang, S. W., Jones, W. L., and Dunn, M. G., "Theoretical and Measured Electron Density Distributions at High Altitudes," *AIAA Journal,* Vol. 11, No. 2, 1973, pp. 141–149.

[12]Zeldovich, Y. B., and Raizer, Y. P., *Physics of Shock Waves and High Temperature Hydrodynamic Phenomena,* Academic, New York, 1966, pp. 407–413.

[13]Makin, B., and Keck, J. C., "Variational Theory of Three-Body Electron Ion Recombination Rates," *Physical Review Letters,* Vol. 11, No. 6, Sept. 15, 1963, pp. 281–283.

[14]Dunn, M. G., "Measurement of $C^+ + e^- + e^-$ and $CO^+ + e^-$ Recombination in Carbon Monoxide Flows," *AIAA Journal,* Vol. 9, No. 11, 1971, pp. 2184–2191.

[15]Dunn, M. G., and Lordi, J. A., "Measurement of $O_2^+ + e^-$ Dissociative Recombination in Expanding Oxygen Flows," *AIAA Journal,* Vol. 8, No. 4, 1970, pp. 614–618.

[16]Dunn, M. G., and Lordi, J. A., "Measurement of $N_2^+ + e^-$ Dissociative Recombination in Expanding Nitrogen Flows," *AIAA Journal,* Vol. 8, No. 2, 1970, pp. 339–345.

[17]Park, C., "Measurement of Ionic Recombination Rate of Nitrogen," *AIAA Journal,* Vol. 6, No. 11, 1968, pp. 2090–2094.

[18]Park, C., "Collisional Ionization and Recombination Rates of Atomic Nitrogen," *AIAA Journal,* Vol. 7, No. 8, 1969, pp. 1653–1654.

[19]Hinnov, E., and Hirschberg, J. G., "Electron-Ion Recombination in Dense Plasmas," *Physical Review,* Vol. 125, No. 3, 1962, pp. 795–801.

[20]Nelson, H. F., and Goulard, R., "Structure of Shock Waves with Nonequilibrium Radiation and Ionization," *Physics of Fluids,* Vol. 12, No. 8, 1969, pp. 1605–1617.

[21]Chapin, C. E., "Nonequilibrium Radiation and Ionization in Shock Waves," Purdue Univ., Lafayette, IN, AA&ES Rept., June 1967.

[22]Foley, W. H., and Clarke, J. H., "Shock Waves Structured by Nonequilibrium Ionizing and Thermal Phenomena," *Physics of Fluids,* Vol. 16, No. 3, 1973, pp. 373–383.

[23]Vinolo, A. R., and Clarke, J. H., "Interrelated Structures of the Transport Shock and Collision Relaxation Layer in a Multitemperature, Multilevel Ionized Gas," *Physics of Fluids,* Vol. 16, No. 10, 1973, pp. 1612–1620.

[24]Zeldovich, Y. B., and Raizer, Y. P., *Physics of Shock Waves and High Temperature Hydrodynamic Phenomena,* Academic, New York, 1966, pp. 382-396, 505-515.

[25]Wilson, J., "Ionization Rate of Air Behind High Speed Shock Waves," *Physics of Fluids,* Vol. 9, No. 10, 1966, pp. 1913–1921.

[26]Carlson, L. A., "Radiative Gasdynamic Coupling and Nonequilibrium Effects Behind Reflected Shock Waves," *AIAA Journal,* Vol. 9, No. 5, 1971, pp. 858–865.

[27]Petschek, H., and Byron, S., "Approach to Equilibrium Ionization Behind Strong Shock Waves in Argon," *Annals of Physics,* Vol. 1, No. 3, 1957, pp. 270–315.

[28]Dix, D. M., "Energy Transfer Processes in a Partially Ionized Two Temperature Gas," *AIAA Journal,* Vol. 2, No. 12, 1964, pp. 2081–2090.

[29]Dix, D. M., "The Governing Macroscopic Equations of Partially Ionized Gases," Aerospace Corporation Rept. TDR-69-2330-04 TN-2, July 1962.

[30]Lee, J. H., "Basic Governing Equations for the Flight Regimes of Aeroassisted Orbital Transfer Vehicles," *Progress in Astronautics and Aeronautics: Thermal Design of Aeroassisted Orbital Transfer Vehicles,* Vol. 96, edited H. F. Nelson, AIAA, New York, 1985, pp. 3–53.

[31]Carlson, L. A., "Radiative Cooling and Nonequilibrium Chemistry Coupling Behind Normal Shock Waves," *AIAA Journal,* Vol. 10, No. 2, 1972, pp. 230–232.

[32]Tiwari, S. N., and Szema, K. Y., "Effects of Precursor Heating on Radiative and Chemically Reacting Viscous Flow Around a Jovian Entry Body," NASA CR-3186, Oct. 1979.

[33]Gupta, R. N., "Navier Stokes and Viscous Shock Layer Solutions for Radiating Hypersonic Flows," AIAA Paper 87-1576, June 1987.

[34]Carlson, L. A., "Approximations for Hypervelocity Nonequilibrium Radiating, Reacting, and Conducting Stagnation Regions," AIAA Paper 88-2672, June 1988.

[35]Carlson, L. A., and Rieper, R. G., "Electron Temperature and Relaxation Phenomena Behind Shock Waves," *Journal of Chemical Physics,* Vol. 57, No. 2, 1972, pp. 760–766.

[36]Carlson, L. A., "Expressions for the Exchange of Energy and Momentum Between Gases at Different Temperatures and Velocities," *Physics of Fluids,* Vol. 13, No. 7, 1970, pp. 1869–1870.

[37]Olstad, W. B., "Nongray Radiating Flow about Smooth Symmetric Bodies," *AIAA Journal,* Vol. 9, No. 1, 1971, pp. 122–130.

[38]Nicolet, W., "User's Manual for the Generalized Radiation Transfer Code (RAD/EQUIL)," NASA CR-116353, Oct. 1969.

[39]Greendyke, R. B., Private Communication, Analytical Methods and Services Corp., Hampton, VA, 1989.

[40]Gnoffo, P. A., Gupta, R. N., and Shinn, J., "Governing Equations and Physical Models for Hypersonic Air Flows in Thermal and Chemical Nonequilibrium," NASA TP-2867, 1989.

[41]Bird, G. A., "Nonequilibrium Radiation During Reentry at 10 km/sec," AIAA Paper 87-1543, June 1987.

[42]Wood, A. D., Hoshizaki, H., Andrews, J. C., and Wilson, K. H., "Measurements of the Total Radiant Intensity of Air," *AIAA Journal,* Vol. 7, No. 1, 1969, pp. 130–139.

[43]Bates, D. R., Kingston, A. E., and McWhirter, R. W. P., "Recombination Between Electrons and Atomic Ions. I. Optically Thin Plasmas," *Proceedings of the Royal Society of London, Series A,* Vol. 267, No. 1330, 1962, pp. 297–312.

[44]Park, C., "Spectral Line Intensities in a Nonequilibrium Nitrogen Plasma," *Journal of Quantitative Spectroscopy and Radiative Transfer,* Vol. 8, No. 10, 1968, pp. 1633–1653.

[45]Park, C., "Comparison of Electron and Electronic Temperatures in Recombining Nozzle Flow of Ionized Nitrogen-Hydrogen Mixture. Part 1. Theory," *Journal of Plasma Physics,* Vol. 9, No. 2, 1973, pp. 187–215.

[46]Kunc, J. A., and Soon, W. H., "Nonequilibrium of High Temperature Nitrogen and Oxygen," AIAA Paper 88-2779, June 1988.

[47]Park, C., "A Review of Reaction Rates in High Temperature Air," AIAA Paper 89-1740, June 1989.